Brightening of Excitons in Carbon Nanotubes on Dimensionality Modification

Yuhei Miyauchi[1,2 *], Munechiyo Iwamura[1], Shinichiro Mouri[1], Tadashi Kawazoe[3], Motoichi Ohtsu[3], and Kazunari Matsuda[1]

[1]*Institute of Advanced Energy, Kyoto University, Uji, Kyoto 611-0011, Japan*

[2]*PRESTO, Japan Science and Technology Agency, 4-1-8 Honcho Kawaguchi, Saitama 332-0012, Japan*

[3]*Department of Electrical Engineering and Information Systems, Graduate School of Engineering, The University of Tokyo, Hongo 7-3-1, Bunkyo-ku, Tokyo 113-8656, Japan*

*email: miyauchi@iae.kyoto-u.ac.jp

Despite the attractive one-dimensional (1D) characteristics of carbon nanotubes[1], their typically low luminescence quantum yield (QY), restricted because of their 1D nature[2-9], has limited the performance of nanotube-based light-emitting devices[10,11]. Here we report the striking brightening of excitons (bound electron–hole pairs)[12,13] in carbon nanotubes through an artificial modification of their effective dimensionality from 1D to 0D. Exciton dynamics in carbon nanotubes with luminescent, local 0D-like states generated by oxygen doping[14] were studied as model systems. We found that the luminescence QY of the excitons confined in the 0D-like states can be more than at least one order larger (~18%) than that of the intrinsic 1D excitons (typically ~1%), not only because of the reduced non-radiative decay pathways but also owing to an enhanced radiative

recombination probability beyond that of intrinsic 1D excitons. Our findings are extendable to the realization of future nanoscale photonic devices including a near-infrared single-photon emitter operable at room temperature.

The low luminescence quantum yield (QY) of semiconducting carbon nanotubes [hereafter, referred as (carbon) nanotubes], which is typically at most only a few percent for dispersed nanotubes[7,8,15-17], is deeply related to their one-dimensional (1D) nature. The balance between radiative and non-radiative relaxation rates (i.e., the probability) of electron–hole bound states, called excitons[12,13], determines the nanotube luminescence QY. Fast non-radiative decay, which dominates the exciton recombination in nanotubes and results in their low luminescence QY, is mainly caused by the quenching of 1D, mobile excitons owing to the rapid collision between these excitons and local quencher states, which include nanotube defects and end sites[4-6,8,9]. Moreover, the temperature (T)-limited radiative relaxation rate ($\propto T^{-1/2}$), characteristic for 1D excitons, substantially reduces the QY at room temperature[2,3,7]. Efforts to improve the luminescence QY by reducing the defect quenching of excitons[18,19] have been reported. Conversely, if a local defect is not an exciton quencher[18-20] but luminescent by virtue of appropriate local electronic structures[14,21-25], the local state may function as a 0D-like quantum state that captures mobile excitons and converts them to photons (as shown in Figure 1) with a radiative relaxation rate possibly lying beyond that of intrinsic 1D excitons. Therefore, 1D nanotubes with luminescent, local 0D-like states offer a unique opportunity for photophysical investigation of nearly ideal 0D–1D hybrid systems. Moreover, understanding the excitonic properties of these states can lead to the development of novel strategies for brightening nanotube excitons beyond the intrinsic limit for future photonics applications.

We examined the excitonic characteristics of luminescent, local 0D-like states embedded in 1D carbon nanotubes. Figure 2(a) shows photoluminescence (PL) excitation maps of carbon nanotubes with and without the doping of oxygen atoms that generate these local states[14]. The distinct luminescence peak at the energy of E_{11}* (~1.07 eV) appears after the oxygen-doping treatment[14] (see Methods and Supplementary Information S1), while the change in the intrinsic luminescence feature at E_{11} (~1.25 eV) is small. The luminescence peak at E_{11}* has been attributed to light emission from the 0D-like local states generated by oxygen doping in carbon nanotubes[14]. The excitation maxima at E_{11} and E_{11}* are coincident with the second sub-band exciton energy E_{22} of (6,5) nanotubes, indicating that the photogenerated intrinsic excitons are converted into local excitons with an energy E_{11}*. Hereafter, we denote the intrinsic exciton state with energy E_{ii} as X_{ii}, and the oxygen-derived local states with energy E_{11}* as X_{11}*. Figure 2(b) compares the absorption spectra of pristine (non-doped) and oxygen-doped nanotubes. The distinct absorption peaks of intrinsic X_{11} and X_{22} excitons of (6,5) nanotubes are almost unchanged, and there are no prominent absorption features originating from the X_{11}* excitons around E_{11}*. The small changes in the absorption spectra indicate that the number density of the X_{11}* sites is very small (deduced to be on the order of one X_{11}* site per micrometer; see Supplementary Information S4), and most parts of the nanotubes except for the oxygen-doped sites remain unchanged.

Figures 2(c)–(h) compare the PL and absorption spectra of various oxygen-doped nanotubes with different X_{11}* peak intensities, which reflect the variable density of the local X_{11}* states. We see a considerable change in the PL spectra of the pristine nanotubes, as shown in Figures 2(c)–(e). As the integrated PL intensity of the

X_{11} peak at E_{11} (I_{11}) slightly decreases, that of the X_{11}* peak at E_{11}* (I_{11}*) emerges and drastically increases.

In Figure 3(a), we plotted the integrated PL intensity of the X_{11}* state, I_{11}*, as a function of the decreasing X_{11} PL intensity ΔI_{11}. Here, ΔI_{11} is defined as $\Delta I_{11} = |I_{11} - I_0|$, where I_0 is the X_{11} PL intensity of the pristine nanotubes. A linear relationship was found to exist between the change in I_{11} (ΔI_{11}) and the value of I_{11}*, as indicated by the dotted, straight line in Figure 3(a), where the slope of the line, I_{11}*/ΔI_{11}, was found to be 7.5 ± 0.6. This linear relation contains rich information on the photophysical parameters of the 0D-like X_{11}* states.

In this study, as shown in Figure 3(b), we consider the migration (diffusion) of the intrinsic 1D excitons along the nanotube and the successive trapping at extrinsic local quenching sites (defect sites), having a density n_q, or at local luminescent sites (X_{11}* sites), having a density of n_x. Based on a 1D diffusion-limited exciton contact-quenching mechanism[8,9] that predicts the luminescence QY η of 1D excitons, where $\eta \propto (n_q + n_x)^{-2}$, the ratio of I_{11}* to ΔI_{11} (for $\Delta I_{11} << I_0$) is evaluated as (see Supplementary Information S2)

$$\frac{I_{11}^*}{\Delta I_{11}} \leq \frac{1}{2}\left(\frac{\eta^*}{\eta_0}\right)\left(\frac{E_{11}^*}{E_{11}}\right), \qquad (1)$$

where η_0 and η^* are the luminescence QYs of an exciton in the X_{11} (non-doped) and X_{11}* states, respectively. Hence, a linear relationship between I_{11}* and ΔI_{11} is expected for small ΔI_{11}. From Eq. 1, a value of $\eta^*/\eta_0 \geq 18 \pm 1$ is derived from the experimental results given in Figure 3(a). That is, the QY of a *single* X_{11}* site is at least ~18 times larger than that obtained from a X_{11} state. Thus, at room temperature, the

luminescence QY of the X_{11}* state, η^*, is estimated to be $\eta^* \geq 18 \pm 6\%$, given that the QY of the X_{11} excitons is $\eta_0 = 1.0 \pm 0.3\%$, as calculated from the reported radiative lifetime of 1.6 ± 0.3 ns[8] and the observed PL decay of X_{11} excitons, as described below (also see Supplementary Information S3).

To clarify the mechanism of the large QY enhancement of the X_{11}* states discussed above, we examined PL decay in pristine and oxygen-doped nanotubes, as shown in Figures 4(a) and (b). Obviously, the PL decay of the X_{11}* excitons at E_{11}* [red solid circles in (b)) is much slower than that of the X_{11} excitons at E_{11}. We conducted a numerical fitting procedure of the intensity decay $I_{11}^{(*)}(t)$ using the stretched exponential function $\exp[-(t/\tau_0)^{1/2}]$ with a characteristic time scale τ_0 for the E_{11} PL decay based on a kinetic model of the diffusion-limited 1D exciton contact quenching[8] and using the double exponential functions for the decay of the 0D-like X_{11}* excitons at E_{11}* (see Supplementary Information S3).

Here, we define a quantity $\langle \tau^{(*)} \rangle = \int_0^\infty I_{11}^{(*)}(t)/I_{11}^{(*)}(0)dt$, which corresponds to the time-integrated exciton number normalized by the initial exciton number and related to η_0 and η^* as $\eta_0 = \tau_R^{-1}\langle \tau \rangle$ and $\eta^* = \tau_R^{*-1}\langle \tau^* \rangle$, respectively, where τ_R and τ_R^* are the radiative lifetimes of the X_{11} and X_{11}* states, respectively. From the fitting procedure (see Supplementary Information S3), the values $\langle \tau \rangle = 16 \pm 4$ ps and $\langle \tau^* \rangle = 95 \pm 7$ ps are obtained. This contributes to the enhancement of the QY of the X_{11}* excitons by a factor of approximately six times that of the intrinsic X_{11} excitons.

The further QY enhancement necessary to account for the net 18× QY enhancement is attributed to the shortened radiative lifetime. Considering the

experimentally estimated values of $\eta^*/\eta_0 \geq 18 \pm 1$ and $\langle\tau\rangle/\langle\tau^*\rangle = 0.17 \pm 0.04 \approx 1/6$, the ratio of the radiative lifetimes can be evaluated through the relation $\tau_R/\tau_R^* = (\eta^*/\eta_0)(\langle\tau\rangle/\langle\tau^*\rangle)$ as $\tau_R/\tau_R^* \geq 3.0 \pm 0.8$, which indicates that the radiative decay rate of the X_{11}* exciton ($1/\tau_R^*$) is approximately more than three times than that of the intrinsic X_{11} excitons ($1/\tau_R$).

Let us now discuss the mechanisms of the reduced non-radiative decay rate, given as a factor of 1/6× (the extended exciton lifetime), and the enhanced radiative decay rate, given as a factor of ≥3× (the shortened radiative lifetime), of the X_{11}* excitons relative to the X_{11} excitons. First, the reduced non-radiative exciton decay is mainly attributed to the exciton immobilization by the localization effect. Once the mobile exciton is *stopped* at a local X_{11}* state, the exciton can avoid collision with quenching sites and live longer, which contributes to the QY enhancement of a factor of about six times. If only this 6× factor enhancement is considered, the QY is evaluated to be 6 ± 2%, which is close to the QY ~ 7% estimated for a clean air suspended nanotube[26].

The dimensionality modification of the excitons is more critical for understanding the further QY enhancement than recovering the original QY of intrinsic 1D excitons. Because of the 1D nature of the intrinsic X_{11} excitons, their effective radiative decay rates are limited by the momentum mismatch between photons and thermally excited excitons in the 1D band dispersion[2,3,7]. This restriction is responsible for the characteristic 1D radiative decay rate that is proportional to $T^{-1/2}$. In contrast, the spatially localized 0D-like states should be free from this momentum restriction, which could lead to enhancement of the radiative decay rate. Considering the possible E_{11}

homogeneous line width of at least 10 meV at room temperature[7], however, the enhancement factor due to this effect is at most 1.6. Hence, to fully explain the enhancement of the radiative decay rate by a factor of 3 ± 0.8, an additional enhancement mechanism of a factor of at least 1.9 ± 0.5 is required.

The remaining issue that should be addressed before we further discuss the enhancement mechanism is whether there is a lower lying dark (optically forbidden) X_{11}* exciton state. If a lower lying dark state exists, the effective radiative decay rate of excitons can be reduced owing to the accumulation of excitons in this dark state, as is actually the case for the intrinsic X_{11} excitons[2,3]. In contrast, if there is no X_{11}* dark state, excitons in the X_{11}* sites can be free from the restriction caused by the dark state and may obtain a larger effective radiative decay rate. To examine the above issue, we conducted temperature-dependent PL studies, as shown in Figures 4(c)–(e). The major findings here are summarized as follows. The temperature-dependent variations of both I_{11} and I_{11}* at the low temperature range shown in Figures 4(d) and (e) are well reproduced by considering the exciton diffusional transport and the reduction of the bright exciton population due to the existence of lower lying dark states not only in the X_{11} states but also in the X_{11}* states, which is consistent with a theoretical prediction for an impurity-bound exciton in carbon nanotubes[27] (see Supplementary Information S5 and S6). From the numerical fitting results, we infer the existence of the X_{11}* dark state, eventually leading to no significant change of the X_{11}* effective radiative decay rate compared to that of the X_{11} excitons at room temperature (see Supplementary Information S6).

Given the negligible change related to the existence of the dark state, we attribute the remaining enhancement of the radiative decay rate by a factor of ~2 to the

increased oscillator strength owing to the squeezing of an exciton in the 0D-like X_{11}* state, which is known as the *giant-oscillator-strength effect* of a localized exciton[28]. The radiative decay rate τ_R^{-1} and the oscillator strength f of an exciton is related as $\tau_R^{-1} \propto E^2 f$, where E is the exciton energy and f is approximately inversely proportional to the average electron–hole separation, i.e., the exciton size in a 1D nanotube. Hence, the radiative decay rate can be enhanced by a factor of ~2 for an exciton squeezed to be ~40% of its original size, considering the different exciton energies E_{11} and E_{11}*. From the size of the X_{11} exciton[29] of ~2 nm in (6,5) nanotubes, the size of the X_{11}* exciton is roughly deduced to be ~0.8 nm.

Our findings regarding the strongly enhanced luminescence properties of sparsely distributed, 0D-like excitonic states beyond the intrinsic properties in 1D carbon nanotubes will stimulate research on the physics of 0D–1D hybrid systems. Furthermore, the findings presented here will allow the development of nanotube-based novel optoelectronic devices while utilizing the advantages of both 0D and 1D electronic systems, such as a near-infrared single-photon emitter[21] driven by direct carrier-injection[30] that can be operated even at room temperature.

Methods

Sample preparation. The oxygen-doped, (6,5) carbon nanotubes dispersed in a D_2O solution used in this work were prepared using ozone in the procedure reported by Ghosh *et al.*[14], but the experimental conditions and parameters were considerably modified so that the broadening of the absorption peak[14], indicating the degradation of the intrinsic part of the nanotubes, could be minimized. Details of the sample preparation procedure are described in Supplementary Information S1. In short,

(6,5)-rich CoMoCAT nanotubes were isolated by dispersion in D_2O with 0.2% (w/v) sodium dodecyl benzene sulfonate (SDBS), 60 min of moderate bath sonication, 40 min of vigorous sonication with a tip-type sonicator, and centrifugation at an acceleration of 130 000 g for 4 h. A 0.75 ml volume of D_2O, containing dissolved ozone with variable density, was added to the resulting 2 ml of isolated nanotube dispersion. For the control samples that are denoted as "pristine" (non-doped) nanotubes, 0.75 ml of D_2O without dissolved ozone was added. The samples were left under a lighted desk lamp (~5 mW/cm^2) typically overnight prior to conducting the optical measurements. In our protocol, the relative oxygen-doping level (number density of the X_{11}* site) was mainly controlled by the density of ozone dissolved in the D_2O solution. The relation between the emerged I_{11}* intensity and the estimated absorbance of ozone at 260 nm in the added D_2O solution is presented in Figure S2. The moderately oxygen-doped nanotubes utilized for the temperature-dependent PL measurements were deposited on a membrane filter and dried in vacuum prior to the measurements. Further details of the sample preparation protocols and parameters are presented in Supplementary Information S1.

Optical measurements and data analysis. Continuous wave absorption and PL spectra of dispersed nanotubes in D_2O were measured at room temperature using a near-infrared spectrometer with monochromated incident light. All the optical measurements at room temperature were conducted on the liquid samples in optical quartz cells. The time-resolved PL decay profiles of the dispersed nanotubes in D_2O were recorded at room temperature using a time-correlated, single-photon counting technique under pulsed laser excitation (80 MHz, ~6 ps pulse duration with a photon energy of 1.378 eV) with a liquid-N_2 cooled near-infrared photomultiplier attached with a microchannel

plate. The PL from each peak feature (E_{11} or E_{11}*) is separated using optical filters with a bandpass of approximately 0.1 eV. The time-resolved measurements were conducted on the same nanotubes for which the PL excitation maps shown in Figure 2(a) were taken. We fitted the data using the convolution of the instrumental response function (IRF) with model functions to obtain the original PL decay profiles (see Supplementary Information S3). Temperature-dependent PL measurements were performed on the as-deposited samples attached to the cold finger of a liquid-He cooled microscopy cryostat, where monochromated light from a broadband light source (Fianium, SC450) was used for the photoexcitation. The measurements were conducted with the excitation energy of 2.175 eV (570 nm), which corresponds to the second sub-band exciton energy E_{22} of (6,5) nanotubes. The PL peaks of the nanotubes casted on a membrane filter were broadened, suggesting a more inhomogeneous environment for the casted nanotubes than that of the micelle-suspended nanotubes. We confirmed that the temperature-dependent variation of the E_{22} exciton energy is sufficiently small by observing the PLE spectra at 5 and 298 K.

References

1. Saito, R., Dresselhaus, G. & Dresselhaus, M. S. *Physical Properties of Carbon Nanotubes* (Imperial College Press, 1998).
2. Perebeinos, V., Tersoff, J. & Avouris, P. Radiative Lifetime of Excitons in Carbon Nanotubes. *Nano Lett.* **5**, 2495-2499 (2005).
3. Spataru, C. D., Ismail-Beigi, S., Capaz, R. B. & Louie, S. G. Theory and Ab Initio Calculation of Radiative Lifetime of Excitons in Semiconducting Carbon Nanotubes. *Phys. Rev. Lett.* **95**, 247402 (2005).
4. Cognet, L. *et al.* Stepwise Quenching of Exciton Fluorescence in Carbon Nanotubes by Single-Molecule Reactions. *Science* **316**, 1465-1468 (2007).
5. Rajan, A., Strano, M. S., Heller, D. A., Hertel, T. & Schulten, K. Length-Dependent Optical Effects in Single Walled Carbon Nanotubes. *J. Phys. Chem. B* **112**, 6211-6213 (2008).
6. Miyauchi, Y., Matsuda, K., Yamamoto, Y., Nakashima, N. & Kanemitsu, Y. Length-Dependent Photoluminescence Lifetimes in Single-Walled Carbon Nanotubes. *J. Phys. Chem. C* **114**, 12905-12908 (2010).
7. Miyauchi, Y., Hirori, H., Matsuda, K. & Kanemitsu, Y. Radiative lifetimes and coherence

lengths of one-dimensional excitons in single-walled carbon nanotubes. *Phys. Rev. B* **80**, 081410(R) (2009).
8. Hertel, T., Himmelein, S., Ackermann, T., Stich, D. & Crochet, J. Diffusion Limited Photoluminescence Quantum Yields in 1-D Semiconductors: Single-Wall Carbon Nanotubes. *ACS Nano* **4**, 7161-7168 (2010).
9. Harrah, D. M. & Swan, A. K. The Role of Length and Defects on Optical Quantum Efficiency and Exciton Decay Dynamics in Single-Walled Carbon Nanotubes. *ACS Nano* **5**, 647-655 (2011).
10. Mueller, T. *et al.* Efficient Narrow-band Light Emission from a Single Carbon Nanotube p-n Diode. *Nature Nanotech.* **5**, 27-31 (2010).
11. Hertel, T. Carbon nanotubes: A Brighter Future. *Nature Photon.* **4**, 77-78 (2010).
12. Ando, T. Excitons in Carbon Nanotubes. *J. Phys. Soc. Jpn.* **66**, 1066-1073 (1997).
13. Wang, F., Dukovic, G., Brus, L. E. & Heinz, T. F. The Optical Resonances in Carbon Nanotubes Arise from Excitons. *Science* **308**, 838-841 (2005).
14. Ghosh, S., Bachilo, S. M., Simonette, R. A., Beckingham, K. M. & Weisman, R. B. Oxygen Doping Modifies Near-Infrared Band Gaps in Fluorescent Single-Walled Carbon Nanotubes. *Science* **330**, 1656-1659 (2010).
15. O'Connell, M. J. *et al.* Band Gap Fluorescence from Individual Single-Walled Carbon Nanotubes. *Science* **297**, 593-596 (2002).
16. Lebedkin, S. *et al.* FTIR-luminescence mapping of dispersed single-walled carbon nanotubes. *New J. Phys.* **5**, 140 (2003).
17. Crochet, J., Clemens, M. & Hertel, T. Quantum Yield Heterogeneities of Aqueous Single-Wall Carbon Nanotube Suspensions. *J. Am. Chem. Soc.* **129**, 8058-8059 (2007).
18. Ju, S.-Y., Kopcha, W. P. & Papadimitrakopoulos, F. Brightly Fluorescent Single-Walled Carbon Nanotubes via an Oxygen-Excluding Surfactant Organization. *Science* **323**, 1319-1323 (2009).
19. Lee, A. J. *et al.* Bright Fluorescence from Individual Single-Walled Carbon Nanotubes. *Nano Lett.* **11**, 1636-1640 (2011).
20. Crochet, J. J., Duque, J. G., Werner, J. H. & Doorn, S. K. Photoluminescence imaging of electronic-impurity-induced exciton quenching in single-walled carbon nanotubes. *Nature Nanotech.* **7**, 126-132 (2012).
21. Högele, A., Galland, C., Winger, M. & Imamoğlu, A. Photon Antibunching in the Photoluminescence Spectra of a Single Carbon Nanotube. *Phys. Rev. Lett.* **100**, 217401 (2008).
22. Hirori, H., Matsuda, K., Miyauchi, Y., Maruyama, S. & Kanemitsu, Y. Exciton Localization of Single-Walled Carbon Nanotubes Revealed by Femtosecond Excitation Correlation Spectroscopy. *Phys. Rev. Lett.* **97**, 257401 (2006).
23. Kilina, S., Ramirez, J. & Tretiak, S. Brightening of the Lowest Exciton in Carbon Nanotubes via Chemical Functionalization. *Nano Lett.* **12**, 2306-2312 (2012).
24. Nagatsu, K., Chiashi, S., Konabe, S. & Homma, Y. Brightening of Triplet Dark Excitons by Atomic Hydrogen Adsorption in Single-Walled Carbon Nanotubes Observed by Photoluminescence Spectroscopy. *Phys. Rev. Lett.* **105**, 157403 (2010).
25. Iakoubovskii, K. *et al.* Midgap Luminescence Centers in Single-wall Carbon Nanotubes Created by Ultraviolet Illumination. *Appl. Phys. Lett.* **89**, 173108 (2006).
26. Lefebvre, J., Austing, D. G., Bond, J. & Finnie, P. Photoluminescence Imaging of Suspended Single-Walled Carbon Nanotubes. *Nano Lett.* **6**, 1603-1608 (2006).
27. Tomio, Y. & Suzuura, H. Aharonov-Bohm Effect on Impurity-bound Excitons in Semiconducting Carbon Nanotubes. *J. Phys: Conf. Ser.* **302**, 012005 (2011).
28. Takagahara, T. & Hanamura, E. Giant-Oscillator-Strength Effect on Excitonic Optical Nonlinearities Due to Localization. *Phys. Rev. Lett.* **56**, 2533-2536 (1986).
29. Luer, L. *et al.* Size and mobility of excitons in (6, 5) carbon nanotubes. *Nature Phys.* **5**, 54-58 (2009).
30. Mizuochi, N. *et al.* Electrically Driven Single-photon Source at Room Temperature in Diamond. *Nature Photon.* **6**, 299-303 (2012).

Acknowledgements

This research was supported by PRESTO (No. 3538 from JST) and by a Grant-in-Aid for Scientific Research (Nos. 24681031, 22740195, and 23340085 from JSPS and No. 22016007 from MEXT). The authors thank Y. Kawazoe, T. Murakami, T. Umeyama, and H. Imahori for experimental equipment and T. F. Heinz for fruitful discussions.

Author contributions

Y.M. developed the concept, designed the experiment and prepared the manuscript. Y.M. and M.I. performed the optical measurements. T.K. and M.O. contributed to the time resolved PL measurements. M.I. prepared the samples. Y.M., M.I., S.M. and K.M. contributed to the interpretation of the results and writing the manuscript. All authors discussed the results and commented on the manuscript.

Additional information

The authors declare no competing financial interests. Supplementary information accompanies this paper at www.nature.com/naturephotonics. Reprints and permission information is available online at http://www.nature.com/reprints. Correspondence and requests for materials should be addressed to Y.M.

Figure Captions

Figure 1 | Schematic of a carbon nanotube with a luminescent, local state. A photoexcited intrinsic exciton is mobile along the nanotube axis (blue spot). When the mobile exciton collides with a local state (red spot), where the exciton energy becomes

lower than that of the intrinsic state, the mobile exciton can be trapped by the local state. If the local state has no efficient non-radiative decay paths, it should work as a luminescence center, and the exciton can decay radiatively by emitting a photon.

Figure 2 | Optical spectra of carbon nanotubes with luminescent, local states. (**a**) PL excitation maps of nanotubes before (pristine) and after (oxygen-doped) the oxygen-doping treatment. The vertical and horizontal axes correspond to the excitation and emission photon energy, respectively. The colors in the map correspond to the PL intensity (white being the highest and black being the lowest). (**b**) Optical absorption spectra of the pristine (black dotted curve) and the oxygen-doped (red solid curve) nanotubes. The vertical dotted line indicates the energy of E_{11}* (~1.07 eV). (**c**)–(**e**) PL spectra of the various nanotubes with variable oxygen-doping measured under the E_{22} energy excitation (2.175 eV). Slight differences observed for the pristine spectra are owing to the use of different batches of starting material. (**f**)–(**h**) Optical absorption spectra of various nanotubes around the E_{11} energy. The PL and absorption spectra with the same background colors [(c, f), (d, g), and (e, h)] were taken from the same nanotubes. In (c)–(h), the black and red solid curves correspond to optical spectra of pristine and oxygen-doped carbon nanotubes, respectively.

Figure 3 | The relationship of luminescence intensities from mobile and local excitons. (**a**) The integrated PL intensity of the X_{11}* peak (I_{11}*) as a function of the absolute value of the change in the PL intensity of the X_{11} peak ΔI_{11}. I_{11}* and ΔI_{11} are normalized by the PL intensity of the X_{11} peak (I_0) of pristine (non-doped) nanotubes. The integrated PL intensities are evaluated by peak decomposition procedures, where

the X_{11}* peak is fit by a Voigt function, and where the weak and broad intensity tail of the lower energy side is not included as I_{11}*. (**b**) A schematic of exciton migration and successive trapping by local quenching sites (including the end sites of nanotubes) with density n_q or by local luminescent (X_{11}*) sites with density n_x.

Figure 4 | Time-resolved and temperature-dependent luminescence studies. Time-resolved PL decay profiles of (**a**) pristine (non-doped) and (**b**) oxygen-doped nanotubes. The blue circles in (a) and (b) indicate the PL decay of X_{11} excitons taken at E_{11} (~1.25 eV) (blue circles), and the red circles in (b) indicate the PL decay at E_{11}* that corresponds to the decay of local X_{11}* states. The gray solid curve is the IRF. (**c**) PL spectra of moderately oxygen-doped nanotubes measured at various temperatures. The temperature-dependent variation of (**d**) I_{11} (blue circles) and (**e**) I_{11}* (red squares). The solid curves in (d) and (e) are reproduced by numerical fitting considering the diffusional transport of X_{11} excitons, exciton trapping at the X_{11}* sites, and the probability that the (d) X_{11} and (e) X_{11}* excitons are in their bright states (calculated by taking into account the lower lying dark states that reside (d) 6.6 meV and (e) 15 meV below the bright states). The dotted curve in (e) is calculated without taking the existence of the lower lying dark state into account (see Supplementary Information S5 and S6).

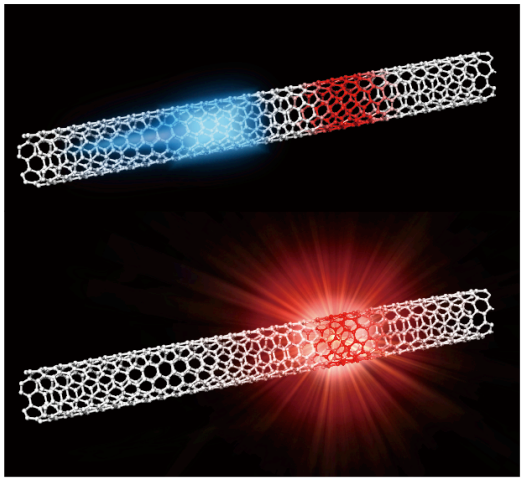

Figure 1. Y. Miyauchi et al.

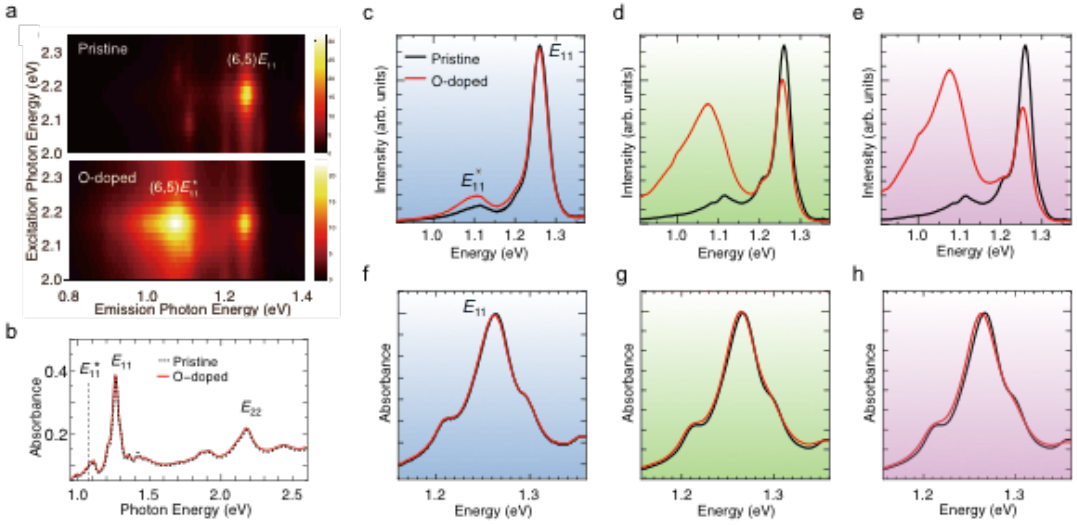

Figure 2. Y. Miyauchi et al.

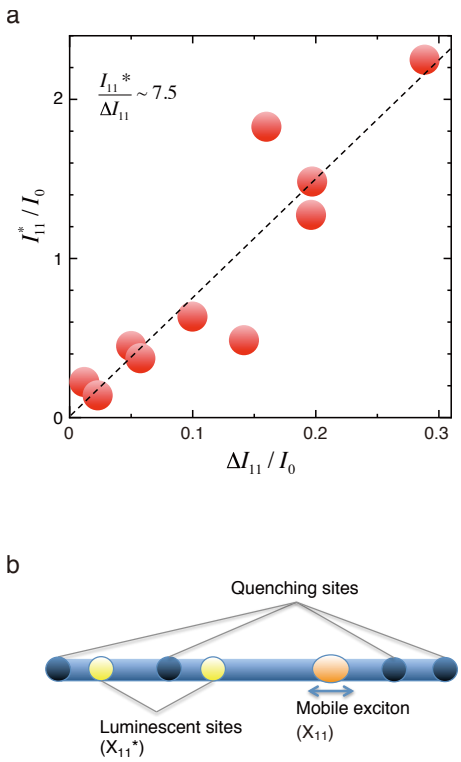

Figure 3. Y. Miyauchi et al.

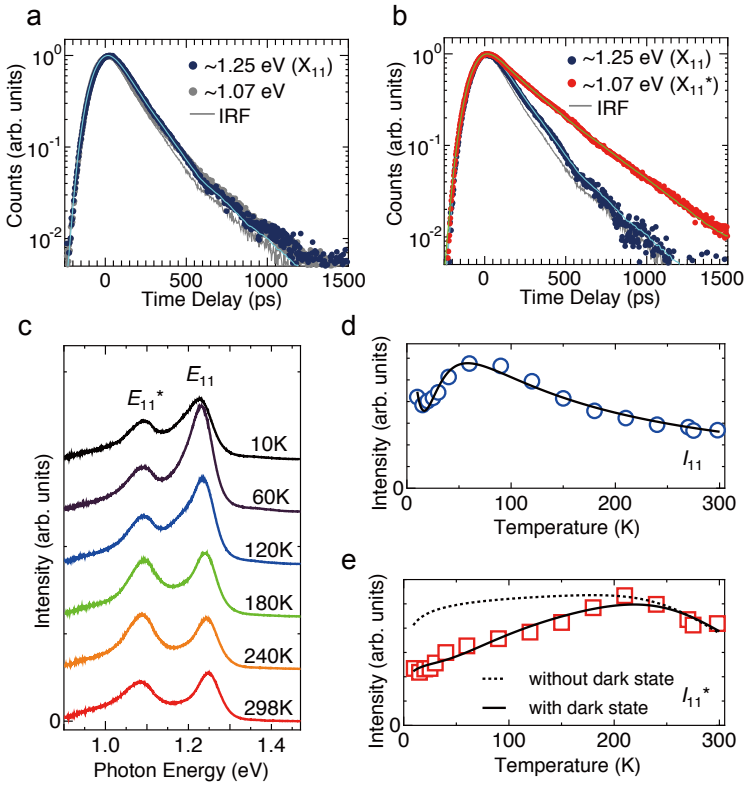

Figure 4. Y. Miyauchi et al.

Supplementary Information

Brightening of Excitons in Carbon Nanotubes on Dimensionality Modification

Yuhei Miyauchi[1,2 *], Munechiyo Iwamura[1], Shinichiro Mouri[1], Tadashi Kawazoe[3], Motoichi Ohtsu[3], and Kazunari Matsuda[1]

[1]*Institute of Advanced Energy, Kyoto University, Uji, Kyoto 611-0011, Japan*

[2]*PRESTO, Japan Science and Technology Agency, 4-1-8 Honcho Kawaguchi, Saitama 332-0012, Japan*

[3]*Department of Electrical Engineering and Information Systems, Graduate School of Engineering, The University of Tokyo, Hongo 7-3-1, Bunkyo-ku, Tokyo 113-8656, Japan*

*email: miyauchi@iae.kyoto-u.ac.jp

S1. Details of the sample preparation procedure

0D-like luminescent X_{11}* states in 1D nanotubes were generated using an oxygen doping method[S1]. In this study, the experimental procedures, conditions, and parameters have been modified from those reported in the pioneering work by Ghosh *et al*.[S1]. The modified procedure is optimized so that the broadening of the absorption peak, indicating the degradation of the intrinsic part of the nanotubes after the oxygen doping procedure, can be minimized.

Figure S1 shows a schematic of the procedure developed in this study for the preparation of low density, oxygen-doped carbon nanotubes. First, 10 mg of (6,5)-rich CoMoCAT nanotubes (#SWeNT Grade S-P95-03 DRY ICH-A004 purchased from

Southwest Nanotechnologies or #SWeNT SG-65 purchased from Sigma Aldrich) were isolated by dispersion in D_2O (#151882-100g purchased from Sigma Aldrich) with 0.2% (w/v) sodium dodecyl benzene sulfonate (SDBS) (#195-07682 purchased from Wako), 60 min of moderate bath sonication, 40 min of vigorous sonication with a tip-type sonicator, and centrifugation at an acceleration of 130 000 g for 4 h. The slight difference in the luminescence spectra of the pristine (non-oxygen-doped) samples shown in Figs. 2(c), (d), and (e) in the main text is because of the fluctuation of the sample preparation conditions depending on the experimental batch; however, the obtained results are consistent with each other.

The D_2O solution with dissolved ozone was prepared by direct bubbling of the ozone gas. A typical optical absorption spectrum of dissolved ozone in D_2O is shown in Fig. S1. First, a high density ozone-dissolved D_2O solution is prepared (absorbance of

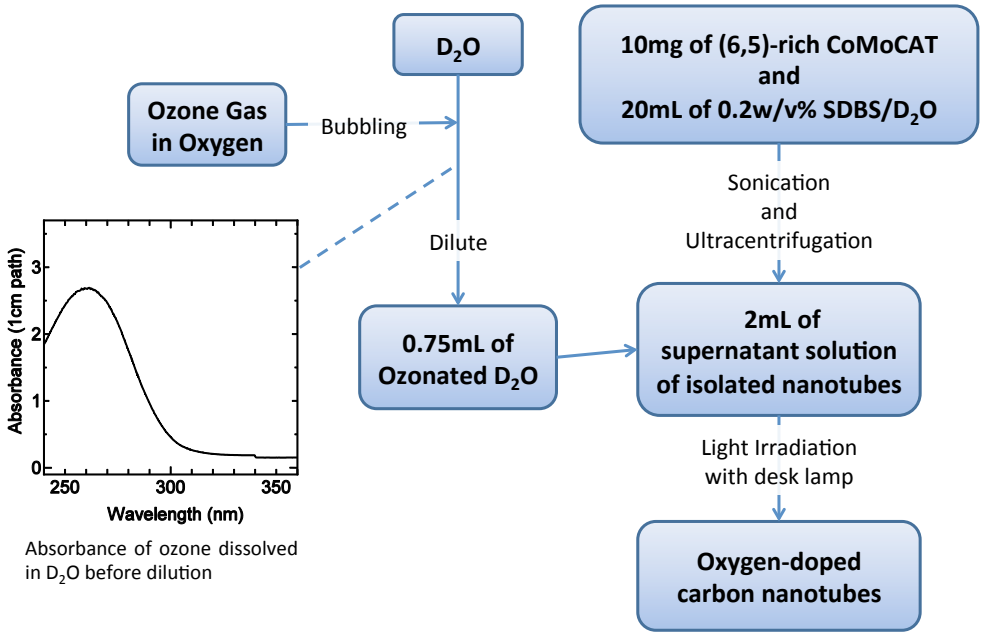

Figure S1 | A schematic of the procedure for low density oxygen doping used in this study.

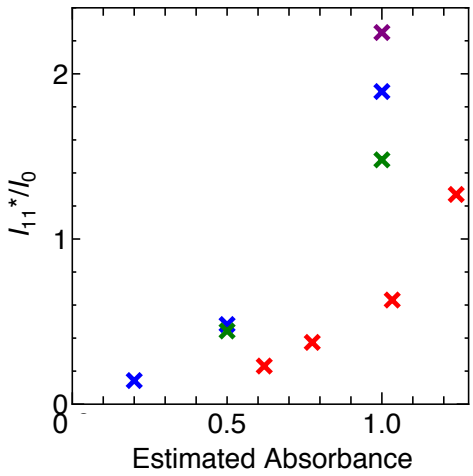

Figure S2 | I_{11}* / I_0 plotted as a function of the estimated absorbance of the added ozone-dissolved D_2O at 260 nm for a 1 cm optical path. Points with the same colors correspond to the same experimental batch.

~3 at 260 nm for a 1 cm optical path), and this solution is diluted to adjust the ozone density. A 0.75 ml volume of ozone-dissolved D_2O, prepared with various dilution ratios, was added to the 2 ml of the isolated nanotube dispersion supernatant. For the control samples that are denoted as "pristine" nanotubes in the main text, 0.75 ml of D_2O without dissolved ozone was added. The samples were left under a lighted desk lamp (~5 mW/cm^2) typically overnight to promote the oxygen doping reaction. Light irradiation is not necessarily required for our oxygen-doping procedure, but it enhances the oxygen-doping level. The oxygen-doping level was controlled by the density of ozone dissolved in the D_2O solution. The relation between the emerged I_{11}* intensity and the estimated absorbance of the ozone-dissolved D_2O at 260 nm used for the oxygen doping is plotted in Fig. S2. The estimated absorbance is calculated from the absorbance of the initial (before dilution) high density ozone-dissolved D_2O and the dilution ratios used for each sample. Although there is fluctuation depending on the experimental batch, it is found that the I_{11}* intensity and the estimated absorbance have basically a positive correlation. Fluctuations depending on the experimental batch are

possibly owing to the unintentional differences in the experimental conditions influenced by the environmental (room) temperature, humidity, and batch of the starting CoMoCAT material.

S2. Evaluation of the ratio of I_{11}* and ΔI_{11}

First, we consider the number of photons N emitted from the X_{11} states, which is related to I_{11} via $N \approx AI_{11} / E_{11}$, where A is a constant. N is proportional to the luminescence QY η and the number of photogenerated X_{11} excitons N_{abs},

$$N = N_{abs}\eta . \tag{S1}$$

Considering the diffusion of photogenerated 1D intrinsic excitons and successive trapping by local luminescent X_{11}* sites, the number of photons emitted from the X_{11}* states N* is expressed as

$$N^* = N_{abs}\left(\frac{k_{dif}}{k_i + k_{dif}}\right)\left(\frac{n_x}{n_q + n_x}\right)\eta^*, \tag{S2}$$

where η* is the luminescence QY of a *single* X_{11}* site, k_{dif} is the effective decay rate of the X_{11} excitons because of exciton diffusion and successive collision with local quenching sites (including local defects) and oxygen-doped sites with densities n_q and n_x, respectively. Only the intrinsic excitons trapped by the X_{11}* sites, with a density n_x, are converted into X_{11}* excitons and emit photons with a QY of η*. The factor k_i is the effective decay rate for all the possible mechanisms of exciton recombination other than diffusion-limited mechanisms. When k_{dif} dominates exciton decay, $k_i << k_{dif}$, and the relationship $k_{dif} / (k_i + k_{dif}) \approx 1$ is expected. Here, we assume that the conversion efficiency Y of an intrinsic exciton to a local exciton at the X_{11}* site is unity. The

discussion remains consistent when the conversion efficiency Y is less than unity, provided n_x is redefined as the *effective* number density of the X_{11}* sites (in this case, the *real* number density of the X_{11}* sites can be obtained as n_x/Y.).

When the luminescence QY η is controlled by the exciton diffusion and successive contact-quenching mechanism, η for non-doped (η_0) and oxygen-doped (η_x) nanotubes are expressed as[S2,S3]

$$\eta_0 \propto \left[\frac{k_{1D}(T)}{D(T)}\right]\frac{1}{n_q^2} \tag{S3}$$

and

$$\eta_x \propto \left[\frac{k_{1D}(T)}{D(T)}\right]\frac{1}{\left(n_q + n_x\right)^2}, \tag{S4}$$

respectively, where $k_{1D}(T) \propto T^{-1/2}$ is the temperature-dependent radiative decay rate of the 1D X_{11} exciton[S4-6], and $D(T)$ is the X_{11} exciton diffusion constant. Using η_0 and η_x, the emitted photon numbers of X_{11} excitons in non-doped (N_0) and oxygen-doped (N_x) nanotubes are expressed as

$$N_0 = N_{abs}\eta_0 \tag{S5}$$

and

$$N_x = N_{abs}\eta_x, \tag{S6}$$

respectively. Using Eqs. (S3)–(S6), the difference in the number of E_{11} photons emitted from the pristine and oxygen-doped carbon nanotubes, $\Delta N \equiv N_0 - N_x$, is evaluated as

$$\Delta N = N_{abs}\eta_0\left(1-\frac{\eta_x}{\eta_0}\right) = N_{abs}\eta_0\left[1-\frac{(n_q+n_x)^{-2}}{(n_q)^{-2}}\right] = N_{abs}\eta_0\left(1+\frac{n_q}{n_q+n_x}\right)\left(\frac{n_x}{n_q+n_x}\right). \tag{S7}$$

Comparing Eq. (S2) and (S7), for the condition of low X_{11}* site density ($n_x << n_q$), we

obtain

$$\frac{N^*}{\Delta N} \approx \frac{1}{2}\left(\frac{\eta^*}{\eta_0}\right)\left(\frac{k_{\mathrm{dif}}}{k_{\mathrm{dif}}+k_{\mathrm{i}}}\right) \le \frac{1}{2}\left(\frac{\eta^*}{\eta_0}\right), \tag{S8}$$

where the factor 2 in Eq. (S8) derives from the expression $1 + [n_q / (n_q+n_x)]$ in Eq. (S7) for the condition of $n_x << n_q$. Finally, considering the relationship between the number of photons and the detected intensity, Eq. (1) in the main text is obtained as

$$\frac{I_{11}^*}{\Delta I_{11}} \le \frac{1}{2}\left(\frac{\eta^*}{\eta_0}\right)\left(\frac{E_{11}^*}{E_{11}}\right). \tag{S9}$$

For $\Delta I_{11} / I_0 = \Delta N / N_0 < 0.2$, which corresponds to the condition of $n_x < 0.12 n_q$, Eq. (S9) is valid within an error of less than 6%.

S3. Analysis of the time-dependent photoluminescence decay

To evaluate the PL decay parameters of X_{11}* excitons, we fit the data using the convolution of the instrumental response function (IRF) with a model double exponential function,

$$I_{11}^*(t) \propto B\exp(-t/\tau_{\mathrm{S}}) + (1-B)\exp(-t/\tau_{\mathrm{L}}) \tag{S10}$$

where B is a positive parameter that is less than 1, and τ_S and τ_L are the short and long time decay constants, respectively. The double exponential function gave a better fit than the single exponential or stretched exponential function, which is possibly because of the inner fine structure of the X_{11}* states, as will be discussed in the following section S6. The very fast initial rise of the PL profile expected for local X_{11}* states was barely resoluble because of the limitation of instrumental time resolution and was therefore neglected. To fit the X_{11} PL decay $I_{11}(t)$, we used the Kohlrausch (stretched exponential) function[S2],

$$I_{11}(t) \propto \exp[-(t/\tau_0)^{1/2}] \qquad \text{(S11)}$$

where τ_0 is the characteristic time scale and is related to the exciton diffusion constant D via the equation $\tau_0 = \pi / (4Dn_q^2)$, which has been derived on the basis of a kinetic model of diffusion-limited exciton contact quenching[S2].

The colored solid curves in Figs. 4(a) and (b) in the main text were obtained by a numerical fitting procedure. The decay parameters thus derived are τ_0 = 8 ± 2 ps (for the X_{11} PL at E_{11} in pristine nanotubes), τ_S = 27 ± 5 ps, τ_L = 290 ± 30 ps, and B = 0.74 ± 0.02 (for the X_{11}* PL at E_{11}* in oxygen-doped nanotubes).

Here, we define a quantity,

$$\left\langle \tau^{(*)} \right\rangle \equiv \int_0^\infty I_{11}^{(*)}(t) / I_{11}^{(*)}(0)\, dt\,, \qquad \text{(S12)}$$

which corresponds to the time-integrated exciton number normalized by the initial exciton number and related to η_0 and η* as $\eta_0 = \tau_R^{-1}\langle\tau\rangle$ and $\eta^* = \tau_R^{*-1}\langle\tau^*\rangle$, where τ_R and τ_R^* are the effective radiative lifetimes of the X_{11} and X_{11}* states, respectively. The factors $\langle\tau\rangle$ and $\langle\tau^*\rangle$ are calculated as $\langle\tau\rangle = 2\tau_0$ and $\langle\tau^*\rangle = B\tau_S + (1-B)\tau_L$. These quantities are generally different from the averaged lifetimes $\bar{\tau} = \int_0^\infty tI(t)\,dt / \int_0^\infty I(t)\,dt$. The time-integrated exciton numbers for the X_{11} and X_{11}* states are evaluated as $\langle\tau\rangle = 16 \pm 4$ ps and $\langle\tau^*\rangle = 95 \pm 7$ ps from the obtained decay parameters, respectively.

S4. Evaluation of the X_{11}* site density n_x

From Eqs. (S3)–(S6), we obtain the relationship between the local quenching site density n_q and the X_{11}* site density n_x as

$$n_{\mathrm{x}} = \frac{1-\sqrt{N_{\mathrm{x}}/N_0}}{\sqrt{N_{\mathrm{x}}/N_0}} n_{\mathrm{q}}, \tag{S13}$$

where N_{x} / N_0 can be obtained from the change in the PL spectra. The factor n_{q} can be estimated from the time-resolved measurement using the relation[S2]

$$n_{\mathrm{q}} = \frac{1}{2}\sqrt{\frac{\pi}{D\tau_0}}. \tag{S14}$$

From Eqs. (S13) and (S14), n_{x} is obtained as a function of D and the experimentally obtained values as

$$n_{\mathrm{x}} = \frac{1-\sqrt{N_{\mathrm{x}}/N_0}}{2\sqrt{D\tau_0/\pi}\sqrt{N_{\mathrm{x}}/N_0}}. \tag{S15}$$

Replacing N_{x} / N_0 by $(I_0 - \Delta I_{11})/I_0$ yields

$$n_{\mathrm{x}} = \frac{1-\sqrt{1-\Delta I_{11}/I_0}}{2\sqrt{(D\tau_0/\pi)(1-\Delta I_{11}/I_0)}}, \tag{S16}$$

where I_0 is the intensity of the X_{11} PL of non-doped (pristine) nanotubes and ΔI_{11} is the absolute value of the difference in the X_{11} PL intensity before and after oxygen doping. Typical D values of the order of 0.1–10 $\mathrm{cm^2/s}$ at room temperature have been reported[S2,S7-9]. Assuming $D \approx 0.1$–10 $\mathrm{cm^2/s}$, the X_{11}* site density n_{x} is ~0.4–4 $\mu\mathrm{m}^{-1}$ for $\Delta I_{11}/I_0 \sim 0.1$, indicating that the number of the X_{11}* sites can be controlled to be of the order of 1 in a single nanotube of micrometer length.

S5. Temperature dependence of the X_{11} PL intensity

Figures 4(c)–(e) in the main text show the results of the temperature-dependent PL studies. Considerably different temperature-dependent changes of the PL intensity were observed from the X_{11} and X_{11}* excitons. As plotted in Fig. 4(d), with increasing

temperature (T), the X_{11} PL intensity exhibits rapid increase and reaches its maximum at $T \sim 60$ K and monotonically decreases for $T > \sim 60$ K. In contrast, the X_{11}* PL intensity plotted in Fig. 4(e) exhibits a monotonic increase with increasing T until reaching its maximum at ~200 K and slightly decreases for $T >$ ~200 K. These temperature-dependent variations of the PL intensity from X_{11} and X_{11}* excitons shown in Figs. 4(c)–(e) can be understood as follows.

First, let us consider the temperature dependence of the X_{11} PL. The temperature-dependent steady-state intensity from X_{11} excitons $I_{11}(T)$ is expressed as

$$I_{11}(T) \propto T^{-1/2} P_{\mathrm{b}}(T) \langle \tau(T) \rangle , \tag{S17}$$

where the factor $T^{-1/2}$ comes from the 1D radiative decay rate and $P_{\mathrm{b}}(T)$ is the probability that an X_{11} exciton is in the bright state during its lifetime. We approximate the temperature dependence of $\langle \tau(T) \rangle$ (as being proportional to η) taking the diffusion-limited exciton decay into account as

$$\langle \tau(T) \rangle \approx \left[k_{\mathrm{dif}}(T) + k_{\mathrm{i}} \right]^{-1} , \tag{S18}$$

where $k_{\mathrm{dif}}(T)$ is the effective decay rate owing to the exciton diffusion and collision with defect quenching sites, and is defined to be proportional to $D(T)(n_{\mathrm{x}}+n_{\mathrm{q}})^2$. The factor k_{i} is a small constant decay rate effectively representing all recombination processes other than the diffusion-limited process. In the diffusion-limited regime where the relationship $k_{\mathrm{i}} << k_{\mathrm{dif}}$ is satisfied, the QY can be simply expressed by Eqs. (S3) and (S4).

The temperature dependence of $\langle \tau(T) \rangle$ thus mainly comes from that of $D(T)$ [being proportional to $k_{\mathrm{dif}}(T)$]. The T dependence of $D(T)$ should depend on the exciton scattering mechanism. In an ideally clean nanotube, the major intrinsic scattering source

for diffusional exciton transport is acoustic phonon scattering. In such a case, an approximately constant value of $D(T)$ is expected, because $D(T) \propto T/\Gamma(T)$ is predicted from the Einstein relation, and the acoustic phonon scattering rate $\Gamma(T)$ itself increases nearly proportional[S10] to T. On the other hand, in a nanotube surrounded by a non-uniform environment, an extrinsic inhomogeneous surface potential may be the dominant scattering source that effectively limits the mean free path ξ of the excitons independent of temperature. For this scattering source, the relationship $D(T) \propto T^{1/2}$ is expected, because $D(T)$ is described as[S11] $D(T) \approx v(T)\xi$, where $v(T)$ is a thermally averaged exciton group velocity proportional to $T^{1/2}$.

In a realistic nanotube, the situation may be in between the above two extreme cases, and the dominant scattering sources for the diffusional transport of excitons should vary depending on the specific surrounding environment. We therefore leave the exponent of T as an empirical parameter, and approximate $k_{\mathrm{dif}}(T)$ as

$$k_{\mathrm{dif}}(T) = k_{\mathrm{dif0}} T^{\alpha}, \qquad \text{(S19)}$$

where α is an exponent depending on the exciton scattering mechanism ($0 \le \alpha \le 0.5$), to be empirically determined by the fitting procedure; the factor k_{dif0} is determined from the experimentally obtained value of $<\tau(T = 300\ \mathrm{K})> \sim 16$ ps.

In addition to the effect of diffusional exciton transport, consideration of the exciton fine structure is also critical toward an understanding of the temperature-dependent PL of carbon nanotubes. To date, intensive theoretical and experimental studies have revealed that the intrinsic exciton PL intensity at low temperature is suppressed because of the existence of a singlet, optically forbidden (dark) exciton state lying several meV below the optically allowed (bright) exciton state

in carbon nanotubes[S4,S5,S12,S13]. This dark state originates from the intrinsic symmetry of the A and B sub-lattice and consequent degeneracy of K and K' valleys in momentum space[S4,S5,S14,S15]. The existence of the dark state with an energy lower than that of the bright state is important because an exciton tends to be in its dark state, especially at low temperature, which effectively reduces the radiative decay rate of the excitons.

The probability that an exciton is in its bright state P_b in Eq. (S17) is obtained from the population ratio of the dark (N_d) and bright (N_b) excitons N_d/N_b as

$$P_b = \frac{1}{1+(N_d/N_b)}. \qquad \text{(S20)}$$

Although N_d/N_b should be a time-dependent quantity in the most rigorous treatment, here we simply approximate N_d/N_b by the steady state solution of the rate equation, taking the finite phonon-assisted scattering rate between the higher (bright) and lower lying (dark) states into account[S13],

$$\frac{N_d(T)}{N_b(T)} = \frac{\exp(\Delta/k_BT)}{1+g\left[\exp(\Delta/k_BT)-1\right]}, \qquad \text{(S21)}$$

where Δ is the energy difference between the bright and dark states and g is a parameter that is proportional to the decay rate of the lower lying state and inversely proportional to the rate constant for the phonon-assisted scattering between the two states. As long as the factor g is substantially less than 1, this simplified treatment can well approximate the time-averaged value of N_d/N_b during the lifetime of the excitons. Setting g = 0 recovers the Boltzmann distribution between the bright and dark exciton states.

The observed variation of I_{11} shown in Fig. 4(d) in the main text is very well reproduced by Eq. (S17) with fitting parameters Δ = 6.6 ± 0.3 meV, g = 0.043 ± 0.006, α = 0.43 ± 0.04 and $k_i \sim (150\ \text{ps})^{-1}$. We obtained a value for the exponent ($\alpha \approx 0.43$)

that is close to 0.5 and well reproduces the observed temperature dependence of I_{11}, implying that the extrinsic scattering mechanisms ($\alpha \approx 0.5$) rather than the intrinsic phonon mechanism ($\alpha \approx 0$) dominate exciton diffusion, as discussed above. Moreover, $\Delta \approx 6.6$ meV, obtained by the fit, is consistent with previous observations[S16,S17] of bright–dark energy splitting obtained through the evaluation of the Aharonov–Bohm effect[S18,S19] in carbon nanotubes. These results suggest that our model, considering both diffusion-limited exciton quenching and the existence of the dark state, successfully predicts exciton physics in carbon nanotubes placed in an arbitrary environment.

S6. Temperature dependence of the X_{11}* PL intensity

Let us then consider the temperature-dependent variation of I_{11}* in Fig. 4(e). In a similar way to Eq. (S17), I_{11}*(T) is expressed as

$$I_{11}^{*}(T) \propto N_{\mathrm{capt}}(T) P_{\mathrm{b}}^{*}(T) \left\langle \tau^{*}(T) \right\rangle . \tag{S22}$$

The factor $N_{\mathrm{capt}}(T)$ is the number of the excitons captured by the 0D-like X_{11}* sites, which may be weakly dependent on the ratio of $k_{\mathrm{dif}}(T)$ and k_{i} as

$$N_{\mathrm{capt}}(T) = N_{\mathrm{abs}} \left[\frac{k_{\mathrm{dif}}(T)}{k_{\mathrm{dif}}(T) + k_{\mathrm{i}}} \right] \left[\frac{n_{\mathrm{x}}}{n_{\mathrm{q}} + n_{\mathrm{x}}} \right] \propto \frac{1}{1 + k_{\mathrm{i}} / k_{\mathrm{dif}}(T)} , \tag{S23}$$

where the values of $k_{\mathrm{dif}}(T)$ and k_{i}, being consistent with the temperature-dependence of I_{11}, should be used. The distinctive difference between Eqs. (S22) and (S17) is the absence in Eq. (S22) of the factor $T^{-1/2}$ of the 1D radiative decay rate, which is not relevant to the 0D states. The factor P_{b}*(T) in Eq. (S22) is the probability that an X_{11}* exciton is in its bright state. If there is no lower lying dark state, the condition P_{b}*(T) = 1 is fulfilled for the entire temperature range. On the other hand, if there is a lower lying

dark state also in the X_{11}* site, as is the case for the X_{11} states, P_b*(T) is approximated by Eqs. (S20) and (S21) with possibly different parameters from those derived for the X_{11} state. From the experimental viewpoint, it has been unclear whether the X_{11}* state has a lower lying dark state, although recent theoretical studies by Tomio and Suzuura[S20,S21] have suggested that there should be a lower lying dark state even for an exciton bound with an impurity potential. We therefore assess both possibilities (with or without a dark state) in the fitting procedure. The ratio of P_b*(T) for the X_{11}* state and P_b(T) for the X_{11} state P_b*(T) / P_b(T) corresponds to the enhancement factor related to the dark exciton effect. P_b*(T) / P_b(T) > 1 suggests an enhancement of the effective radiative decay rate in the X_{11}* state. Conversely, P_b*(T) / P_b(T) ≤ 1 indicates that there is no radiative decay enhancement related to the dark exciton effect.

In addition to the behavior of I_{11}* at the lower temperature range, we observed a reduction of I_{11}* for T > ~200 K, as shown in Fig. 4(e) in the main text. The reduction of I_{11}* in the higher temperature range can be understood as an Arrhenius-type quenching[S22,S23] behavior that reduces $\langle \tau^*(T) \rangle$ for T > ~200 K as

$$\langle \tau^*(T) \rangle \propto \frac{1}{1 + C \exp(-E_a / k_b T)} \tag{S24}$$

where E_a is the activation energy corresponding to the energy needed to promote the X_{11}* exciton into the original 1D X_{11} state, such that $E_a = E_{11} - E_{11}^* \sim 180$ meV. The factor C is a constant related to the phonon scattering rate-constant and the lifetime of the X_{11}* exciton, and is treated as a fitting parameter. Equation (S24) expresses exciton escape from the local X_{11}* site to the 1D X_{11} state owing to thermal activation, where optical phonon modes with the energies of ~170–200 meV in carbon nanotubes, which are relevant to the so-called G-mode observed in Raman spectra[S24], are available to

promote the X_{11}* exciton into the X_{11} state.

The solid and dotted curves shown in Fig. 4(e) in the main text are calculated using Eqs. (S22)–(S24). For the solid curve in the figure (labeled as "with dark state"), the existence of a lower lying dark state for the X_{11}* site and a finite scattering rate between the bright and dark states are assumed, where P_b*(T) is calculated using Eqs. (S20)–(S21). For the dotted curve in the figure (labeled as "without dark state"), P_b*(T) = 1 is assumed regardless of T, corresponding to the condition that there is no lower lying dark state or no scattering to the dark state.

The observed variation of I_{11}* shown in Fig. 4(e) is very well reproduced by the fitting procedure, taking into account a lower lying dark state with parameters $\Delta^* = 15 \pm 4$ meV and $g^* = 0.27 \pm 0.04$, implying that the local X_{11}* site also has the dark state. The fit results suggest that the bright–dark energy splitting for the local X_{11}* exciton is more than two times larger than that ($\Delta \approx 6.6$ meV) of the intrinsic 1D excitons. From the parameters obtained by the fitting procedure, $P_b^* / P_b \sim 1$ at room temperature is calculated, suggesting that the impact of the existence of the dark state on the enhancement of the X_{11}* radiative decay rate is eventually small.

Let us now discuss the validity of the analysis and the obtained parameters from the numerical fitting. According to the theoretical predictions[S20,S21], the bright–dark energy splitting for an ideal impurity-bound exciton in a carbon nanotube depends on the spatial range x of the impurity potential compared with the lattice constant a. For $x < a$ (a short range impurity potential), Δ^* is predicted to be larger than Δ for the intrinsic exciton because inter-valley scattering by the short range impurity potential is possible and the scattering matrix element for the bright and dark excitons

are different. Hence, we attribute the large Δ^* for the X_{11}^* exciton to additional inter-valley scattering owing to the short range impurity potential introduced by the doped oxygen atom. An increased bright–dark energy splitting $\Delta^* - \Delta$ of the order of 10 meV is in a reasonable range predicted for an impurity potential placed at one carbon site[S20].

We then examine the validity of the parameter $g^* \approx 0.27$. The parameter g^* (corresponding to g in Eq. (S21)) is expressed as $g^* = \Gamma_D^*/\gamma_0^*$, where Γ_D^* is the decay rate of the lower lying dark exciton. The factor γ_0^* is the scattering rate-constant, which determines phonon-assisted upward ($\gamma\uparrow^*$) and downward transition ($\gamma\downarrow^*$) rates[S13]. Within the three level (bright, dark, and ground levels) model that yields Eq. (S21)[S13], the time-dependent X_{11}^* bright exciton decay becomes a double exponential function[S25], which we actually observed in the time-dependent PL study shown in Fig. 4(b) in the main text. By comparing the time-dependent solution of the rate equations with the experimental decay curve obtained from the fitting procedure (see Supplementary Information S3), the decay rate of the bright (Γ_B^*) and dark (Γ_D^*) X_{11}^* excitons and the scattering rate constant γ_0^* at room temperature, $\Gamma_B^* \approx (117\ \text{ps})^{-1}$, $\Gamma_D^* \approx (851\ \text{ps})^{-1}$, and $\gamma_0^* \approx (115\ \text{ps})^{-1}$, are deduced. We can therefore compare the value of $g^* = \Gamma_D^*/\gamma_0^*$ deduced from the time-dependent X_{11}^* PL with that derived from the temperature dependence. From the above deduced decay parameters, $g^* \approx 0.14$ is obtained, which is of the same order of magnitude as $g^* \approx 0.27$ obtained from the temperature-dependent PL intensity. Despite the different sample conditions (micelle-suspended or dried in vacuum), the results from the time-dependent and temperature-dependent studies are thus reasonably consistent with each other.

Finally, we summarize the discussions in sections S5 and S6. We observed considerably different temperature dependencies of the PL intensity for X_{11} and X_{11}* excitons. The different temperature-dependent variations can be consistently reproduced by considering (i) the difference in the dimensionality of the X_{11} (1D) and X_{11}* (0D) excitons, (ii) diffusional transport of X_{11} excitons and exciton capturing by (and escaping from) the local sites, and (iii) the existence of lower lying dark states for both X_{11} and X_{11}* exciton states. Based on the analysis described above, we infer that there is a lower lying dark exciton state of the X_{11}* exciton and that the existence of the dark state is not related to the significant enhancement of the radiative decay rate of the X_{11}* exciton compared to that of the X_{11} exciton.

Supplementary References

S1. Ghosh, S., Bachilo, S. M., Simonette, R. A., Beckingham, K. M. & Weisman, R. B. Oxygen Doping Modifies Near-Infrared Band Gaps in Fluorescent Single-Walled Carbon Nanotubes. *Science* **330**, 1656-1659 (2010).

S2. Hertel, T., Himmelein, S., Ackermann, T., Stich, D. & Crochet, J. Diffusion Limited Photoluminescence Quantum Yields in 1-D Semiconductors: Single-Wall Carbon Nanotubes. *ACS Nano* **4**, 7161-7168 (2010).

S3. Harrah, D. M. & Swan, A. K. The Role of Length and Defects on Optical Quantum Efficiency and Exciton Decay Dynamics in Single-Walled Carbon Nanotubes. *ACS Nano* **5**, 647-655 (2011).

S4. Perebeinos, V., Tersoff, J. & Avouris, P. Radiative Lifetime of Excitons in Carbon Nanotubes. *Nano Lett.* **5**, 2495-2499 (2005).

S5. Spataru, C. D., Ismail-Beigi, S., Capaz, R. B. & Louie, S. G. Theory and Ab Initio Calculation of Radiative Lifetime of Excitons in Semiconducting Carbon Nanotubes. *Phys. Rev. Lett.* **95**, 247402 (2005).

S6. Miyauchi, Y., Hirori, H., Matsuda, K. & Kanemitsu, Y. Radiative Lifetimes and Coherence Lengths of One-dimensional Excitons in Single-walled Carbon Nanotubes. *Phys. Rev. B* **80**, 081410(R) (2009).

S7. Cognet, L. *et al.* Stepwise Quenching of Exciton Fluorescence in Carbon Nanotubes by Single-Molecule Reactions. *Science* **316**, 1465-1468 (2007).

S8. Miyauchi, Y., Matsuda, K., Yamamoto, Y., Nakashima, N. & Kanemitsu, Y. Length-Dependent Photoluminescence Lifetimes in Single-Walled Carbon Nanotubes. *J. Phys. Chem. C* **114**, 12905-12908 (2010).

S9. Rajan, A., Strano, M. S., Heller, D. A., Hertel, T. & Schulten, K. Length-Dependent Optical Effects in Single Walled Carbon Nanotubes. *J. Phys. Chem. B* **112**, 6211-6213 (2008).

S10. Matsuda, K., Inoue, T., Murakami, Y., Maruyama, S. & Kanemitsu, Y. Exciton Dephasing and Multiexciton Recombinations in a Single Carbon Nanotube. *Phys. Rev. B* **77**, 033406 (2008).

S11. Crochet, J. J. *et al.* Disorder Limited Exciton Transport in Colloidal Single-Wall Carbon Nanotubes. *Nano Lett.* **12**, 5091-5096 (2012).

S12. Mortimer, I. B. & Nicholas, R. J. Role of Bright and Dark Excitons in the Temperature-Dependent Photoluminescence of Carbon Nanotubes. *Phys. Rev. Lett.* **98**, 027404 (2007).
S13. Matsunaga, R., Miyauchi, Y., Matsuda, K. & Kanemitsu, Y. Symmetry-induced Nonequilibrium Distributions of Bright and Dark Exciton States in Single Carbon Nanotubes. *Phys. Rev. B* **80**, 115436-115436 (2009).
S14. Zhao, H. & Mazumdar, S. Electron-Electron Interaction Effects on the Optical Excitations of Semiconducting Single-Walled Carbon Nanotubes. *Phys. Rev. Lett.* **93**, 157402 (2004).
S15. Ando, T. Effects of Valley Mixing and Exchange on Excitons in Carbon Nanotubes with Aharonov–Bohm Flux. *J. Phys. Soc. Jpn.* **75**, 024707 (2006).
S16. Matsunaga, R., Matsuda, K. & Kanemitsu, Y. Evidence for Dark Excitons in a Single Carbon Nanotube due to the Aharonov-Bohm Effect. *Phys. Rev. Lett.* **101**, 147404 (2008).
S17. Srivastava, A., Htoon, H., Klimov, V. I. & Kono, J. Direct Observation of Dark Excitons in Individual Carbon Nanotubes: Inhomogeneity in the Exchange Splitting. *Phys. Rev. Lett.* **101**, 087402 (2008).
S18. Ajiki, H. & Ando, T. Aharonov-Bohm Effect in Carbon Nanotubes. *Physica B: Condensed Matter* **201**, 349-352 (1994).
S19. Ando, T. Excitons in Carbon Nanotubes. *J. Phys. Soc. Jpn.* **66**, 1066-1073 (1997).
S20. Tomio, Y. & Suzuura, H. Impurity-induced Valley Mixing of Excitons in Semiconducting Carbon Nanotubes. *Physica E: Low-dimensional Systems and Nanostructures* **42**, 783-786 (2010).
S21. Tomio, Y. & Suzuura, H. Aharonov-Bohm Effect on Impurity-bound Excitons in Semiconducting Carbon Nanotubes. *J. Phys: Conf. Ser.* **302**, 012005 (2011).
S22. Andersen, O. K. & Veje, E. Experimental Study of the Energy-band Structure of Porous Silicon. *Phys. Rev. B* **53**, 15643-15652 (1996).
S23. Valenta, J., Bruhn, B. & Linnros, J. Coexistence of 1D and Quasi-0D Photoluminescence from Single Silicon Nanowires. *Nano Lett.* **11**, 3003-3009 (2011).
S24. Saito, R., Dresselhaus, G. & Dresselhaus, M. S. *Physical Properties of Carbon Nanotubes* (Imperial College Press, 1998).
S25. Berciaud, S., Cognet, L. & Lounis, B. Luminescence Decay and the Absorption Cross Section of Individual Single-Walled Carbon Nanotubes. *Phys. Rev. Lett.* **101**, 077402 (2008).